# We are IntechOpen, the world's leading publisher of Open Access books Built by scientists, for scientists

6,900
Open access books available

185,000
International authors and editors

200M
Downloads

Our authors are among the

154
Countries delivered to

TOP 1%
most cited scientists

12.2%
Contributors from top 500 universities




WEB OF SCIENCE™

Selection of our books indexed in the Book Citation Index in Web of Science™ Core Collection (BKCI)

## Interested in publishing with us?
## Contact book.department@intechopen.com

Numbers displayed above are based on latest data collected.
For more information visit www.intechopen.com



Chapter 8

# Droplet Impact and Evaporation on Nanotextured Surface for High Efficient Spray Cooling

Cheng Lin

Additional information is available at the end of the chapter

http://dx.doi.org/10.5772/51826

## 1. Introduction

Resulting from Moore's law in semiconductor technology, the progresses such as shrinking feature size, increasing transistor density, and improving circuit speeds, lead to higher chip power dissipations and heat fluxes. Consequently, new and novel cooling techniques are of interest. Bar-Cohen et al. [1] have reviewed several techniques for direct liquid cooling, such as pool boiling, gas-assisted evaporative cooling, jet impingement, spray cooling and synthetic jets, emphasizing the important implications of a direct liquid approach in the thermal management of hot spots, where heat fluxes can be as high as 1~2 kW/cm$^2$. Nanotubes have unique properties as discussed by Berber et al. [2] are reported to have measured high thermal conductivities around 6600 W/mK at room temperature for carbon nanotubes. These can be placed in the thermal interface material to provide a low heat resistance path through the thermal interface material, significantly improving the thermal conductivity of the TIM. Two-phase heat transfer involving the evaporation of a liquid in a hot region and the condensation of the resulting vapor in a cooler region can provide large heat fluxes needed for microelectronic packages to operate at acceptable temperature levels. Spray cooling, which involves the boiling of a working fluid on a heated surface, is an example of efficient heat transfer scheme that exploit the benefits of two-phase heat transfer. Nanotextured surfaces provide new opportunities to improve the controllable fluid and heat transport for thin film evaporation. Significant efforts in previous work focused on spray cooling of microstructured surfaces [3,4] and the employment of nano-textured surfaces to achieve an enhanced boiling heat transfer [5]. Carbon nanotubes (CNTs) forests have more recently been investigated to enhance nucleate boiling and film boiling [6]. Four regimes have been identified: flooded, thin film, partial dry-out and dry-out. The heated surfaces of micro-structure are most suited in the thin film and partial dry-out regimes because of the

INTECH
open science | open minds

© 2012 Lin, licensee InTech. This is an open access chapter distributed under the terms of the Creative Commons Attribution License (http://creativecommons.org/licenses/by/3.0), which permits unrestricted use, distribution, and reproduction in any medium, provided the original work is properly cited.

wetting enhancement. Sodtke and Stephan [7] demonstrated that micro-structured surfaces lead to an increased contact line length and thereby increase the overall heat flux. The proposed enhanced boiling mechanism is the integration of spray cooling on nanotextured surfaces, which is expected to improve the heat transfer coefficient over 10 times (up to 1000 W/cm$^2$). Numerous studies have been proposed cooling methods using spray cooling and pooling boiling with nanostructure have achieved very high heat fluxes; they are listed in Table 1 [8-13]. Amon *et al.*[8] and Hsieh and Yao[9] studied the heat transfer on square microstuds (160~480 mm size, groove depths 333~455 μm, groove widths 120~360 μm) manufactured on silicon. Two full-cone pressurized spray nozzles (60° and 80° cone angles, flow rates up to 4.41 g/cm$^2$ min, $d_{32}$ between 75 and 100 μm) were used to spray water at very low flow rates onto the surfaces. Surface texture was found to have little effect in the single-phase and dryout regimes. The authors attributed the higher heat transfer observed for the microtextured silicon surfaces in the intermediate regimes to more effective spreading of the liquid by capillary forces. A plain aluminum surface was found to have higher heat transfer than a silicon surface, but this disadvantage could be overcome by surface texturing. The maximum heat flux achieved was just over 50 W/cm$^2$. Visaria and Mudawar [10] developed a relatively new universal CHF correlation that combines the spray inclination functions and corrected subcooling constant. The CNT coating, the parallel vertical CNTs as well as the mesh of CNTs create deep, near-zero-angle cavities that are ideal for embryo formation, especially for the low contact angle coolants. Ujereh *et al.*[11] also demonstrated significant CHF enhancement with CNTs for both silicon and copper walls because of the aforementioned increase in surface area. Li *et al.* [12] fabricated Cu nanorods having 50 nm diameter and 450 nm height using oblique-angle deposition. In a pool boiling experiment of water, the wall superheat was decreased, and the CHF was improved by about 10% compared to a flat Cu surface. The authors showed that multiple scales from nano to micro play a key role in enhancing the nucleate boiling performance. Chen *et al.* [13] synthesized Cu and Si nanowires by electroplating Cu into nanoscale pores and aqueous electroless etching (EE) techniques respectively. The pool boiling experiments with water showed more than 100% increase in the CHF value. The present work focuses on pool boiling of saturated water on nanowires, made of Si or Cu, and observe significant enhancement of both critical heat flux and thermal conductance on nanowires compared to plain surface. The reported CHF (~200 W/cm$^2$) is among the highest values for pool boiling heat transfer.

The remarkable boiling heat transfer performance of the proposed scheme is mainly attributed to the following four characteristics: (1) the large latent heat of vaporization which makes boiling a very efficient mode of heat transfer, (2) the nanostructures which achieve higher cooling performance in the thin film and partial dry-out regime, because more water will be retained on the heat transfer surface due to the capillary force, (3) the enhancement in critical heat flux (CHF) which is realized by the increase of boiling area on nano- textured surfaces, and (4) the super-hydrophilic nano-textured surface which is expected to result in much higher evaporative heat transfer rate. Recently, we have demonstrated manipulation schemes that can passively drive water droplets undergoing

spontaneous self-directed motion upon contact with a chemically patterned nano-textured surface (nano-wetting effect) and with a surface tension gradient [14,15]. As such, small droplets can be transported at high rates to quickly remove dissipated heat from the surface. Following the presentation of a recent conference paper [16], this work proposes enhanced boiling mechanism is the integration of spray cooling on nanotextured surfaces, which is expected to improve the heat transfer coefficient over multiple times.

| Reference | Working fluid | Droplet size | Heater size | Dominant heat transfer mechanism | Critical Heat Flux (CHF) |
|---|---|---|---|---|---|
| 2005 ASME JHT (Amon et al.) [8] | HFE-720 | 50~100 μm | 25.2×25.2 $mm^2$ | Spray cooling (Evaporation and boiling) | 45 $W/cm^2$ |
| 2006 IJHMT (Hsieh et al.) [9] | Water | 75~100 μm | 25.2×25.2 $mm^2$ | Spray cooling (Evaporation and boiling) | 50 $W/cm^2$ |
| 2009 IEEE CPAT (Visaria and Mudawar) [10] | Water, FC-72, FC-77, FC-87 and PF-5052 | 111~249 μm | 10×10 $mm^2$ | Spray cooling (Evaporation and boiling) | 100 $W/cm^2$ |
| | | Nanowire size/ Contact angle(CA) | | | |
| 2007 IJHMT (Ujereh et al.) [11] | FC-72 | 50 nm(dia.) 20~30 μm(height) Very small CA | 12.7×12.7 $mm^2$ | Pool boiling (Nucleate Boiling) | ~30 $W/cm^2$ |
| 2008 Small (Li et al.) [12] | Water | 40~50 nm (dia.) 450 nm(height) CA=38.5 ° | 10×10 $mm^2$ | Pool boiling (Nucleate Boiling) | ~160 $W/cm^2$ |
| 2009 Nano Letter (Chen et al.) [13] | Water | 200 nm(dia.) 40~50 μm(height) CA～0 ° | 10×10 $mm^2$ | Pool boiling (Nucleate Boiling) | ~200 $W/cm^2$ |

**Table 1.** Summary of previous works on evaporation/boiling on micro/nano-structure coated surface

## 2. Experiment set-up and procedure

Deionized water impinging on solid surface was studied by recording the impingement process with a high speed camera at 2000 frames/s. A schematic of the experiment set-up is shown in figure 1. The component include the following: droplet generation system, nano-textured surface and heating system, high-speed charged coupled device (CCD) camera (Ultima APX Fastcam, Photron Ltd., Japan) and lighting system. All components were synchronized so as to achieve simultaneous droplet imaging and thermal measurements.

The water droplets used in the experiment had diameter of ~2 mm and velocity of ~0.3 m/s. Three different impingement surfaces were used: an oxidized silicon, a vertical CNTs and curved CNTs surface. The range of diameters and lengths of the CNTs is about 57~105 nm and 4.28~8.48 μm, respectively. In table 2, the detail specification of the growth of CNTs on the silicon substrate, and test section are presented.

MWCNTs have been synthesized on Ni/Ti multilayered metal catalysts by thermal CVD at 400 °C, in which acetylene was used as carbon source in a 3-inch diameter quartz tube of the furnace. The Ni/Ti multilayered metal catalysts were found to decrease CNT growth temperature effectively. We used a temperature ramp to 800 ◎ at a rate of 20 ◎/min with a constant argon flow rate of 400 sccm (standard cubic centimeter per minute). At the stable temperature, followed by Ar (200 sccm) and $NH_3$ (200 sccm) were added to the furnace for 10 minutes. Finally, the chip cooled down at a rate 5 °C/ min. The coating thickness and nanowire size were measured with a micrometer and shown in an SEM images. Figure 2 shows the cross sectional view of the carbon nanotubes coated surface. The as-grown CNTs are superhydrophobic with a measured contact angle as high as 146°. The carbon nanotubes were functionalized using two methods: (1) $H_2O$ plasma was utilized during the treatment, the flow rate of $H_2O$ plasma was set at 1 sccm with duration of 30 sec.(2)aqueous solution of 6M $H_2SO_4$ at 80°C for 1 hour as shown in Figure 3. Water contact angle measurement using a FTA200 system (First Ten Angstroms Inc.) indicated the contact angle of 4.7°±1.0° (superhydrophilic) for the vertical CNTs surfaces and the contact angle of 1.1°±0.3° (superhydrophobic) for the curved CNTs surfaces. This functionalization of CNTs is superhydrophilic with a measured contact angle as low as 5° are shown in Figure 4.

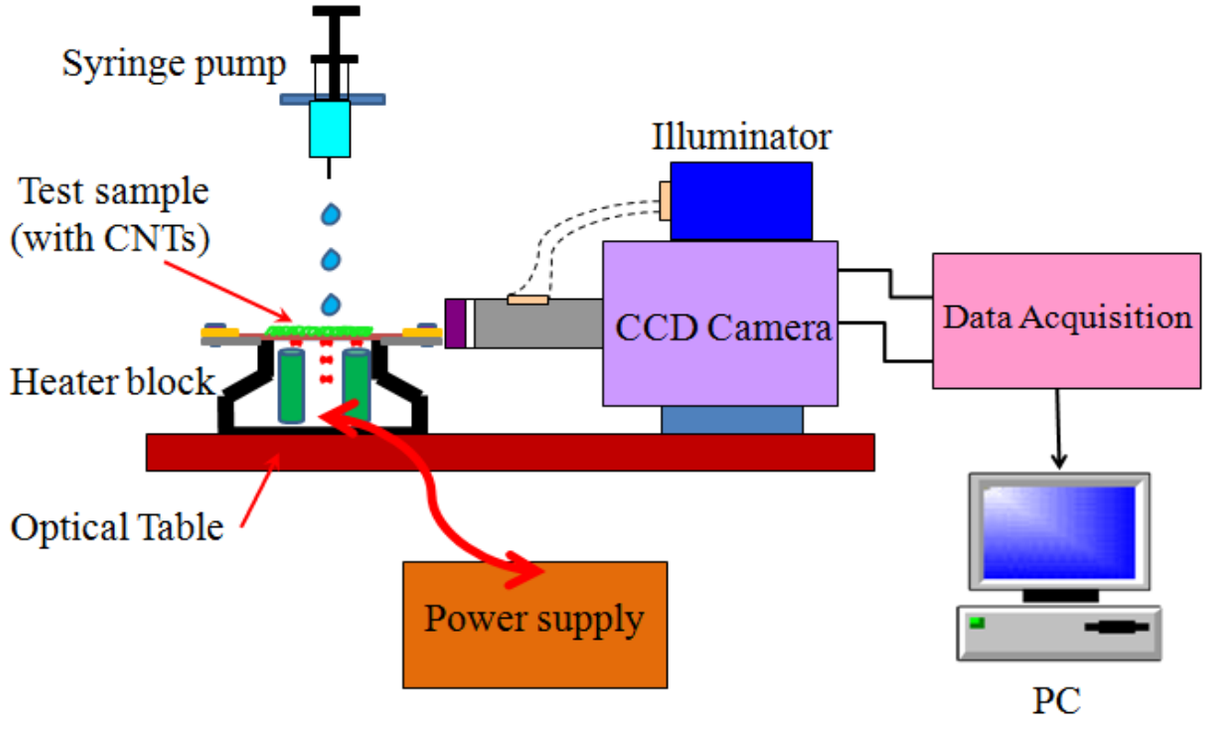



**Figure 1.** Schematic of an experimental apparatus.

| Type / Parameter | Vertical CNTs | Curved CNTs |
|---|---|---|
| Height h(μm) | 7.28~8.48 | 4.28~7.14 |
| Diameter D(nm) | 70.9~92.1 | 57.3~105.4 |
| Silicon substrate W×L×H (mm) | 10×10 ×0.4 | 10×10×0.4 |

**Table 2.** The structural parameter of test sections

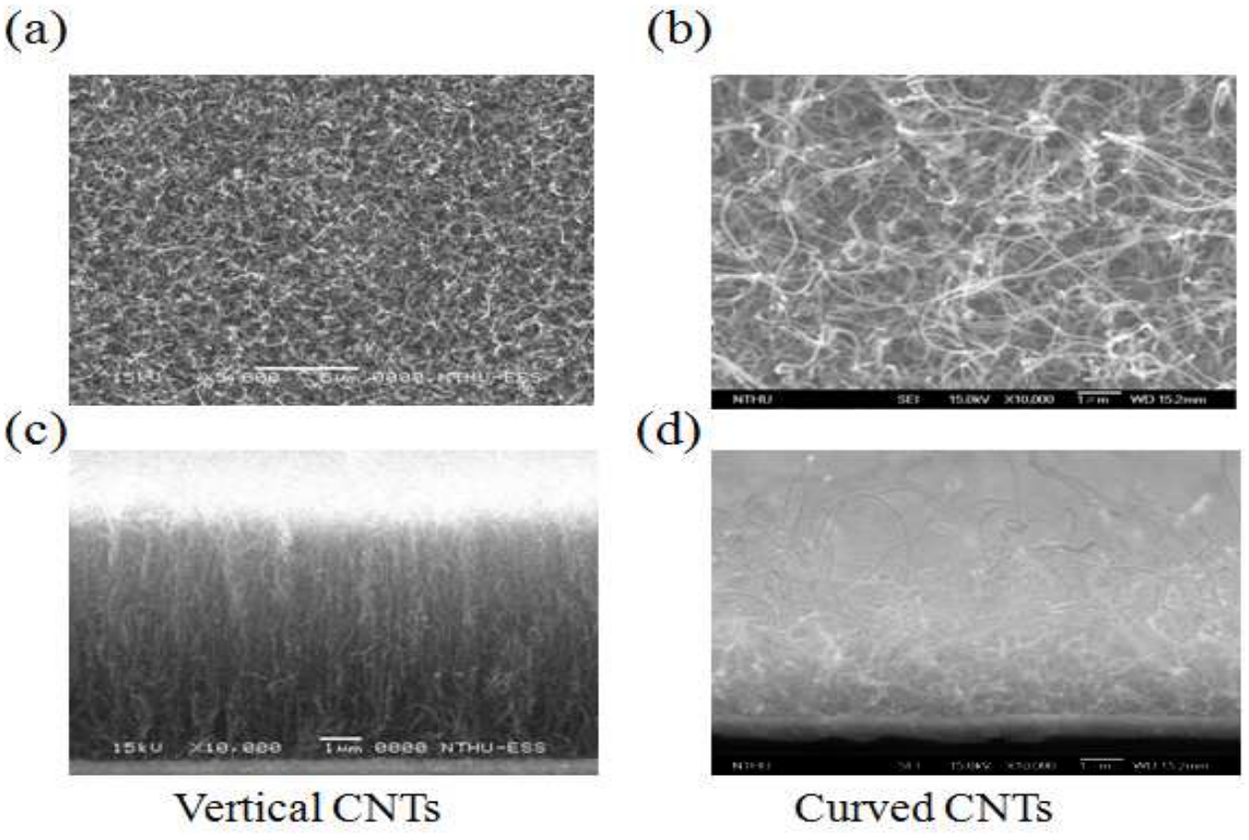



**Figure 2.** SEM images of the different testing surfaces:(a) top view of the vertical CNTs,(b) top view of the curved CNTs, (c)side view of the vertical CNTs, (d) side view of the curved CNTs.

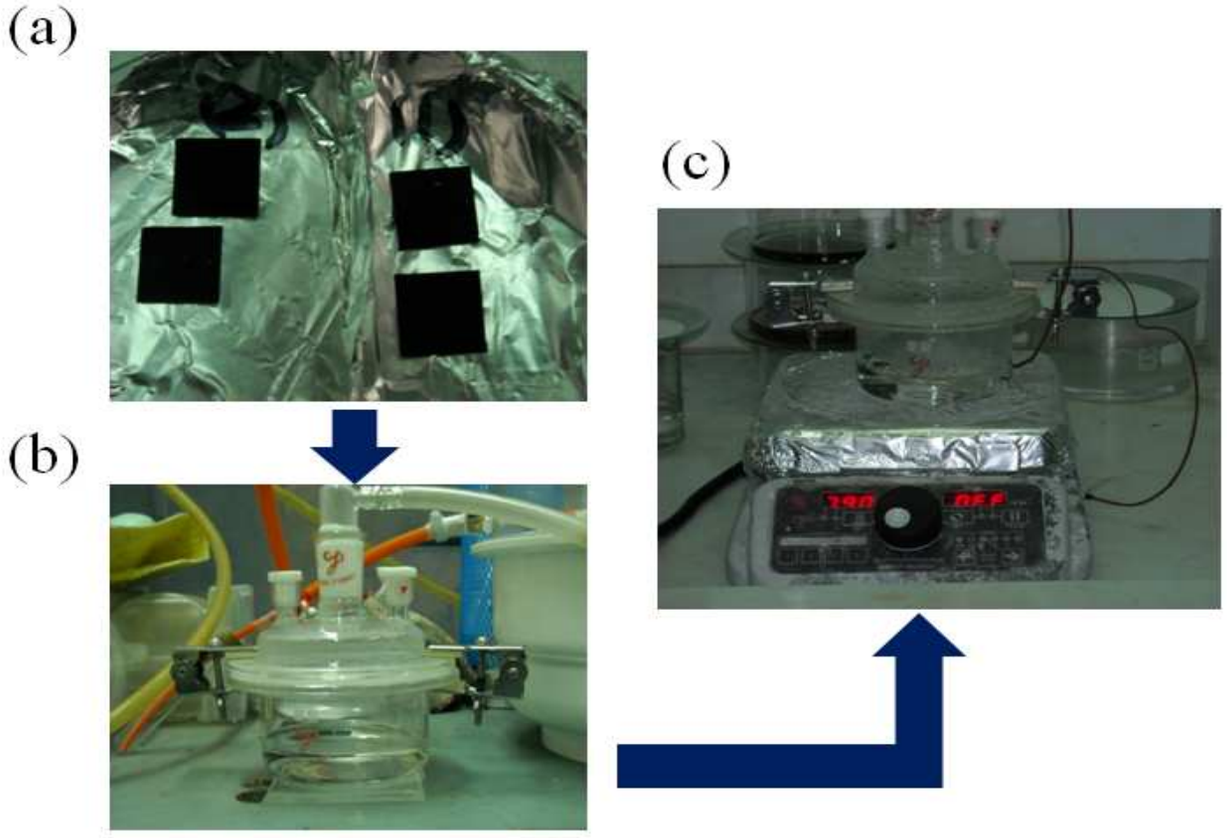



**Figure 3.** Schematic of the samples with CNTs surface treatment sequence: (a) top view of the CNTs samples,(b) vacuum for 5minutes using pump, (c) 80 °C, $H_2SO_4$ solution for 1hr.

The heat flux and the heat transfer coefficient of the heated surface were evaluated with the temperature difference ($\Delta T$), by measuring the mean temperature between the surrounding temperature around the heated surface and the wall temperatures read by the thermocouples in the copper block. The heat flux is obtained as follows,

$$q'' = \frac{IV}{A} = h(T_s - T_a) = h\Delta T \tag{1}$$

Note that the heat transfer coefficient in Eq. 1 can also be written in the form

$$h = \frac{q''}{(T_s - T_a)} \tag{2}$$

where q" is the heat flux (W/cm$^2$), I is the current (Ampere), V is the voltages, and A is the heating surface area of the heated surface. The total amount of heat supplied to the heater was measured by using a power meter system, and the data for all temperatures and powers were recorded by using a data acquisition system. Heat flux was regulated successively by changing the voltage input through the DC power supply. When steady state was reached (the variation of $\Delta T$ in the range of approximately 0.2 °C), all required data were stored, and the next step was executed at a higher voltage.

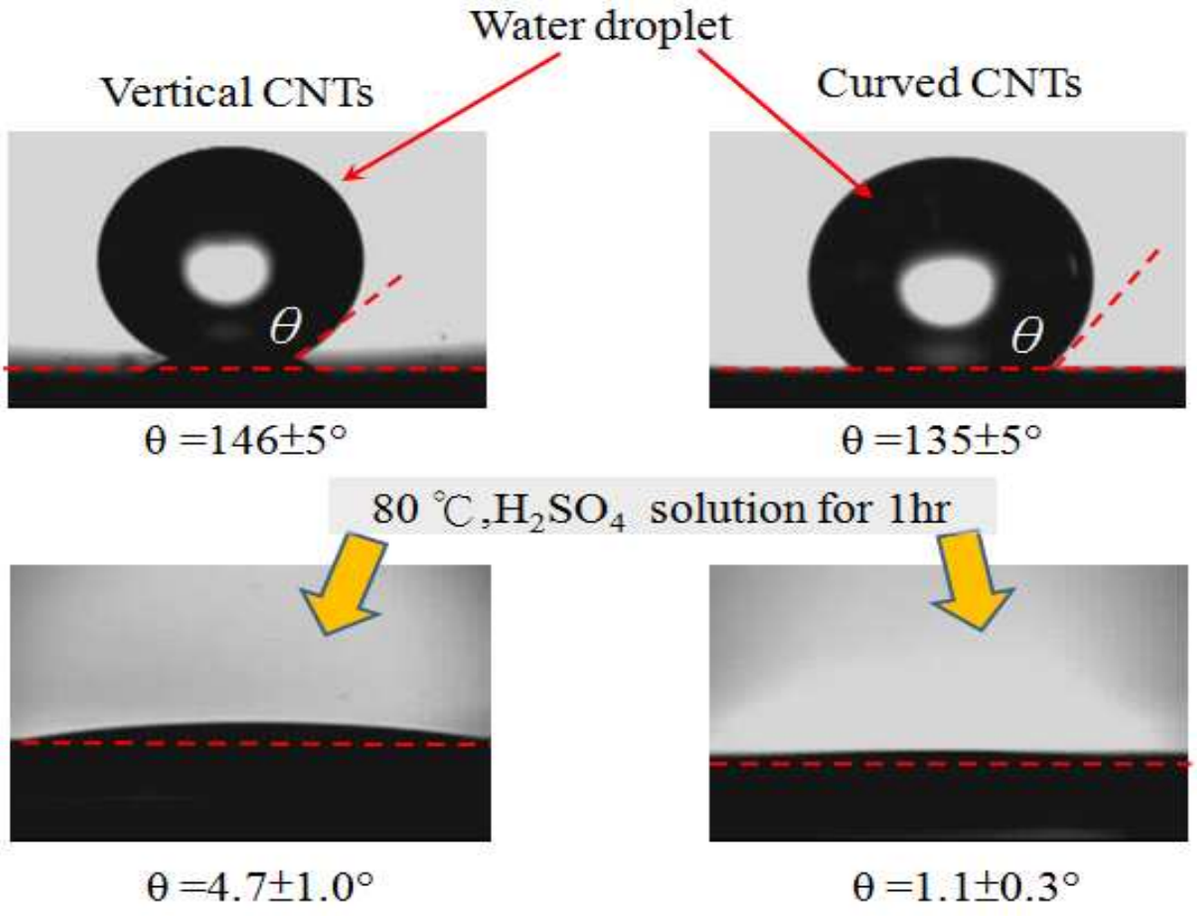



**Figure 4.** The contact situations of water droplets on carbon nanotubes surfaces without (upper row) and with (bottom row) $H_2SO_4$ treatment

## 3. Theoretical model

One aspect of spray cooling is basic boiling phenomena, which should be considered as a prerequisite to the more complex process of spray cooling. Therefore, consider boiling in the absence of an incoming spray. Boiling is a highly efficient means of heat transport in which liquid is vaporized due to the temperature of the liquid exceeding the saturation vapor pressure. In boiling, heat can be removed by increasing the temperature of the liquid (sensible heating) as well as the vaporization process (latent heating). As shown in Figure 5 [17], the boiling curve is a plot of surface heat flux versus excess surface temperature above saturation. When a preheated alloy exits the die in an extrusion, forging, or continuous casting process, it is typically at a temperature above the Leidenfrost point (D point) and the surface experiences film boiling. This boiling regime is characterized by a thermally-insulating layer of steam forming between the surface and individual impinging drops, resulting in poor heat transfer. When the Leidenfrost temperature is reached, the vapor film is interrupted by partial contact of liquid with the surface, causing the surface heat flux to increase with decreasing temperature until the point of critical heat flux (C point: CHF). After CHF, the surface is cooled by nucleate boiling until the temperature falls into the

single-phase regime. Spray cooling is preferred to quenching in stagnant liquid because it raises the Leidenfrost temperature and enhances significantly the heat transfer rate even in the film boiling regime.

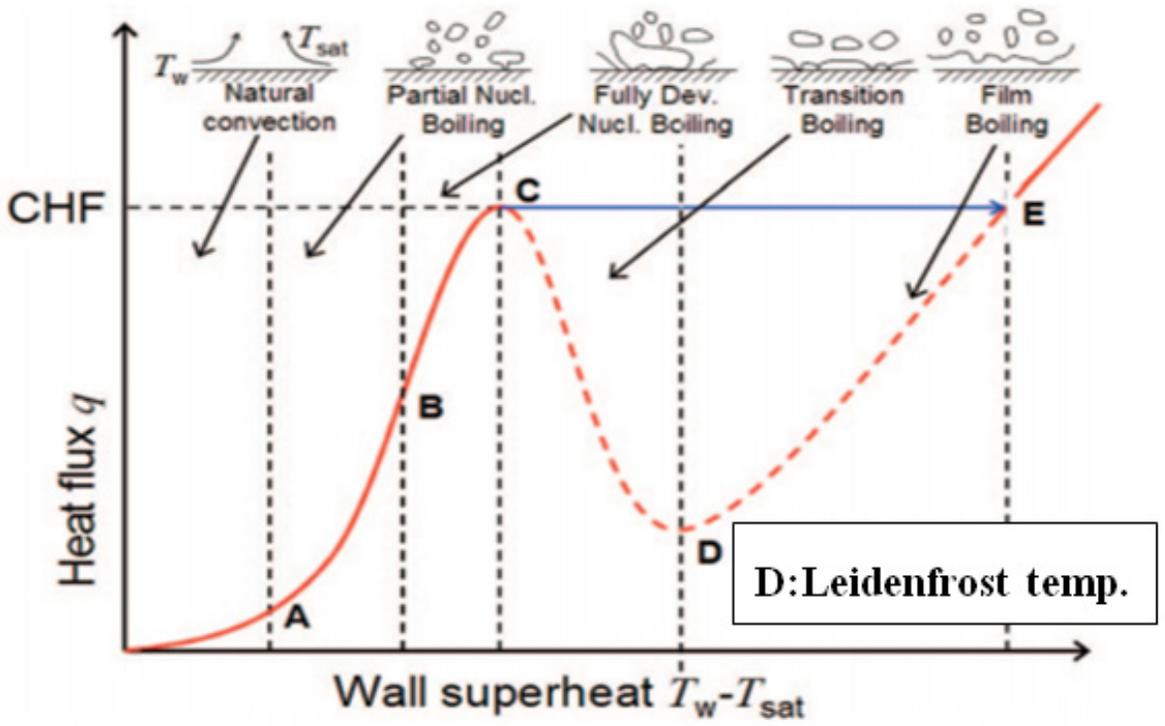



**Figure 5.** Typical boiling curve and associated boiling regimes showing heat flux vs. wall superheat ($T_w$ - $T_{sat}$ ) (adapted from ref. 17)

### 3.1. Impinging droplets on wetting surface modeling

The dynamics of droplet impact on the two types CNTs surfaces modified by aqueous solution of 6M $H_2SO_4$ at 80°C for 1 hour were characterized to demonstrate how the surface energy influences drop impact transitions from bouncing to wetting. The antiwetting pressure ($P_A$) and wetting pressure ($P_w$) influenced the wetting states of impinging droplets. When Pw was larger than Pa, the droplet struck the surface in a wetting state. The wetting pressure (Pw) is given by

$$P_W = \frac{1}{2}\rho V^2 \tag{3}$$

where ϱ and V are the density and the velocity of the impinging liquid, respectively. For nanotextured surface, the antiwetting pressure is capillary pressure. The maximum value of $P_A$ is calculated as the Laplace pressure of the maximum deformation of the water-air interface between posts of nanostructures, the capillary pressure is defined as

$$P_A = -2\sqrt{2}\gamma_{lv}\cos\theta_A / D \tag{4}$$

where $\gamma_{lv}$ is the surface energy of the water at the liquid-vapor interface (0.073 N/m), $\theta_A$ is the advancing CA of the water droplet on the flat surface, and D is the spacing between the nanoscale posts of the nanostructure surface. However, this model has limitations in that only two wetting states are available: bouncing or wetting. Thus, for example, the wetting state of a droplet partially pinned at the contact area cannot be sufficiently explained by these two pressures. A new wetting pressure, the effective water hammer pressure($P_e$) at the contact stage, is therefore introduced. At the moment of impact on the nanostructure, the compressed region of the droplet with pressure ($P_e$) pushes on the liquid-air interface between the nanoposts and induces the penetration of liquid in the contact area. The maximum possible $P_e$ for a spherical droplet impinging at low impact speed is defined by

$$P_e \approx 0.2\rho CV \tag{5}$$

where C is the speed of sound in water (1497 m/s). When $P_A$ is smaller than Pe but larger than Pw, the droplet is in a partial wetting state. The water droplets used in the experiment had diameters of ~2 mm and velocity of ~0.3 m/s. A high-speed camera (up to 4 K frames/s) was used in the study. Relative magnitude of the wetting and antiwetting pressures decides the wetting states of impinging droplets: (1) total wetting state ($P_e$>$P_W$>$P_A$) as water penetrates in both contact and spreading stage.(2) partial wetting state($P_e$> $P_A$ >$P_W$) as water penetrates only during contact stage.(3) Total nonwetting state ($P_A$ > $P_e$> $P_W$) as the structure resist wetting in both stages [18]. In this experiment the droplet completely wetting state within the modified CNTs surfaces, with penetration of water in both contact and spreading stages.

### 3.2. Key parameter of evaporative spray cooling

The surface enhancement is realized by an array of square pins. The microstructures on the heating surface not only increase the heat transfer area but also provide a driving force for liquid spreading. To characterize the capillary force between micro-pins, a dimensionless parameter, Bond number ($B_O$), be expressed as

$$Bo = \frac{G}{\sqrt{\gamma / (\rho_l - \rho_v)g}} \tag{6}$$

The Bond number was defined as the ratio of the gravitational force to the surface tension force. Generally, narrower grooves (smaller G; smaller $B_O$) are more desirable in evaporative heat transfer because of the better liquid spreading ability. Hence, there may exist on an optimal groove width for the evaporative water spray cooling on enhanced silicon surfaces. Another influential surface factor in current study is the bottom surface area of the grooves, because it is directly related to the surface area available for the liquid evaporation in the grooves.

Several control parameters that influence on the impact dynamics include: droplet size, liquid viscosity μ, and impact velocity $V_0$ .We describe these effects in terms of dimensionless numbers: the Weber number $We_d$, the ratio of kinetic energy to surface energy, characterizing the deformability of the droplet; the Reynolds number Re, the ratio of inertia to viscosity effect:

$$We_d = \frac{\rho_f V_0{}^2 d}{\sigma};\ \mathrm{Re}_d = \frac{\rho_f V_0 d}{\mu} \tag{7}$$

Here d the diameter of the liquid drop, $V_0$ is the impact velocity, ϱ is the liquid density, σ is the surface tension, and μ is the liquid viscosity.

At wetting heat transfer, the droplets can be in continuous or semi-continuous direct contact with heat surface. After an initial period of transient conduction heat transfer, the droplets enter into either nucleate or transition boiling regimes. In this case, the droplet incoming Weber number may have a week effect on enhancing the droplet breakup. Wet (hydrophilic surface) cooling results in a significant drop in the surface temperature due to its highly cooling efficiency. In non-wet cooling, also referred to as film boiling, a significant amount of water vapor is generated between the heat surface and the droplet, thus preventing direct contact. Since vapor has a very low thermal conductivity, it acted as insulation between the surface and the incoming spray; therefore, lower cooling efficiency. In this boiling regime, the impact droplet velocity (or Weber number) has a significant influence on the cooling efficiency. For low Weber number, droplets cannot penetrate through the film layer. For high Weber number, droplets can penetrate through the film layer, and more surface contact can be established. The impact velocity for this case is ~30 cm/s and the corresponding Weber number ($We_d$) is 2.47.

### 3.3. Empirical model of evaporative spray cooling

In spray cooling, empirical models have been developed with the continuous expansion of experimental data based on system of interests. Mudawar and Estes (19) first attempted an empirical model to predict CHF in spray cooling by correlating CHF with the volumetric flux of liquid and the Sauter Mean Diameter of droplets, as following:

$$\frac{q_{CHF}}{\rho_v h_{lv} V} = 1.467\left[(1+\cos(\frac{\theta}{2}))\cos(\frac{\theta}{2})\right]^{0.3}\left[\frac{\rho_l}{\rho_v}\right]^{0.3}\left[\frac{\rho_l V^2 d_{32}}{\sigma}\right]^{-0.35}\left[1+0.0019\frac{\rho_l C_{pl}\Delta T_{sub}}{\rho_v h_{lv}}\right] \tag{8}$$

where $\theta$ is the spray cone angle, $d_{32}$ is the Sauter Mean Diameter, $\sigma$ is the surface tension, $\Delta T_{sub}=T_{sat}-T_l$ is liquid subcooling at nozzle inlet, V is average volumetric flux over spray impact area, and $h_{lv}$ is the evaporative latent heat. To predict CHF using Eq.(8), the nozzle parameters and droplet parameter (pressure drop across the nozzle, volumetric flow rate, inclined angle, and Sauter Mean Diameter of droplets) have to be tested. In addition, the distance between the nozzle orifice and the heated surface needs to be chosen carefully, so that the spray cone exactly covers the heated surface. This model was validated by a set of experiments of the spray cooling on a rectangular 12.7×12.7 $mm^2$ flat surface using refrigerants (FC-72 and FC-87). The volumetric flow rate was regulated inside the range of (16.6~216)×$10^3$ $m^3 \cdot s^{-1}/m^2$. The Sauter Mean Diameter of droplets was inside the range of 110~195 μm. The superheat temperature was below 33 °C. The accuracy of this model was claimed to be within ±30%.

Fluid flow for droplet impact was modeled using a finite-difference solution of the Navier–Stokes equations in a three-dimensional Cartesian coordinate system. The liquid is assumed to be incompressible and any effect of the ambient air on droplet impact dynamics is neglected. The fluid flow is assumed to be laminar. The free surface of the deforming droplet is tracked using the volume of fluid (VOF) method which solves the time-dependent Navier-Stokes equations, and interface evolution equation to simulate a mixture of two immiscible fluids with surface tension described in [20].

## 4. Results and discussion

During the entire impingement process, the droplet goes through impact, advancing, maximum spreading, receding and a period of oscillation with pinned contact line. For the non-heating ($T_s$=24°C) case once the oscillation decrease the drop gradual equilibrium at a 55°contact angle on oxidized silicon surface in Figure 6(a). Figure 6(b) shows time sequence images of a water droplet falling on superhydrophilic surface. Figure 6 indicates the different droplet dynamics variables. From the figure 7 prior to impact, the droplet diameter ($d_0$) and impact velocity ($V_0$) were measured. The time is determined to be zero at the moment of impact and the spreading time can be calculated relative to the impact time.

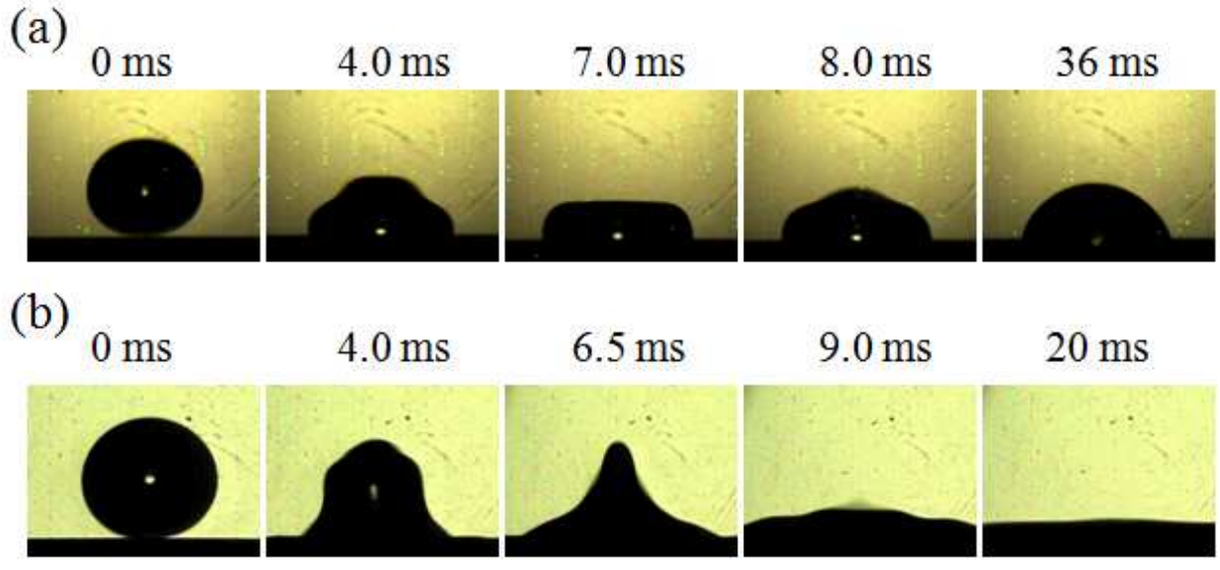
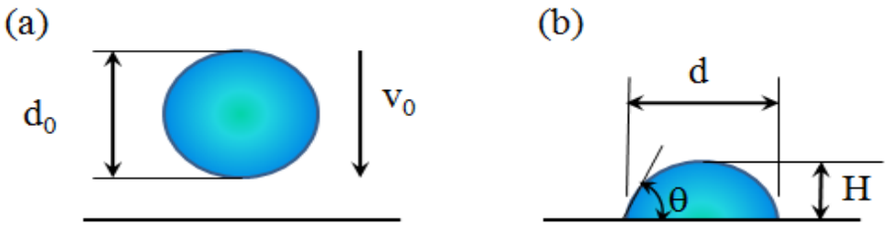



**Figure 6.** Illustration of droplet dynamic impinging process : (a )on the oxidized flat surface, (b)on hydrophilic curved-CNTs surface.

Images of a typical impingement with boiling process are shown in figure 8, where (a)-(e) are the images corresponding to the five stages listed. During initial impact, the droplet rapidly spreads, rebounds and then oscillates at a near-constant wetting diameter. Boiling involves initial nucleation followed by severe boiling including droplet ejection and expansion, and evaporative cooling with the absence of boiling. At non-boiling heating levels the droplet experiences evaporation once the oscillation period ends. Droplet height decreases while the wetting diameter remains nearly constant. When a critical angle is reached, the droplet diameter diminishes rapidly and then dry-out occurs.




| Parameter | Non-dimensional |
|---|---|
| $d^*$ | $d/d_0$ |
| $H^*$ | $H/d_0$ |
| $t^*$ | $t/(d_0/V_0)$ |

**Figure 7.** Droplet hydrodynamics parameters: (a) pre-impact, (b) post-impact

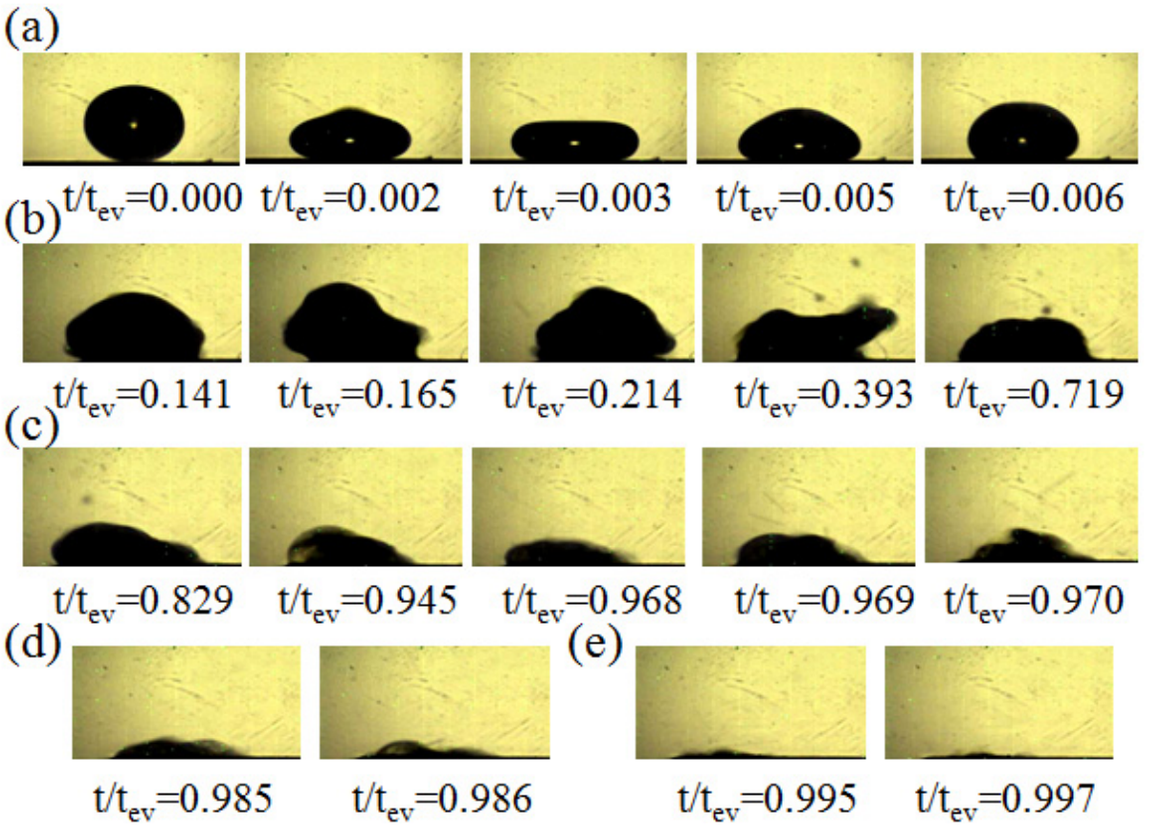



**Figure 8.** Droplet images of the five stages of impingement process for water impinging on the curved CNTs surface at Ts = 187°C: (a) initial impact, (b) boiling, (c) near-constant wetting diameter evaporation, (d) fast receding contact line evaporation, (e) final dry-out

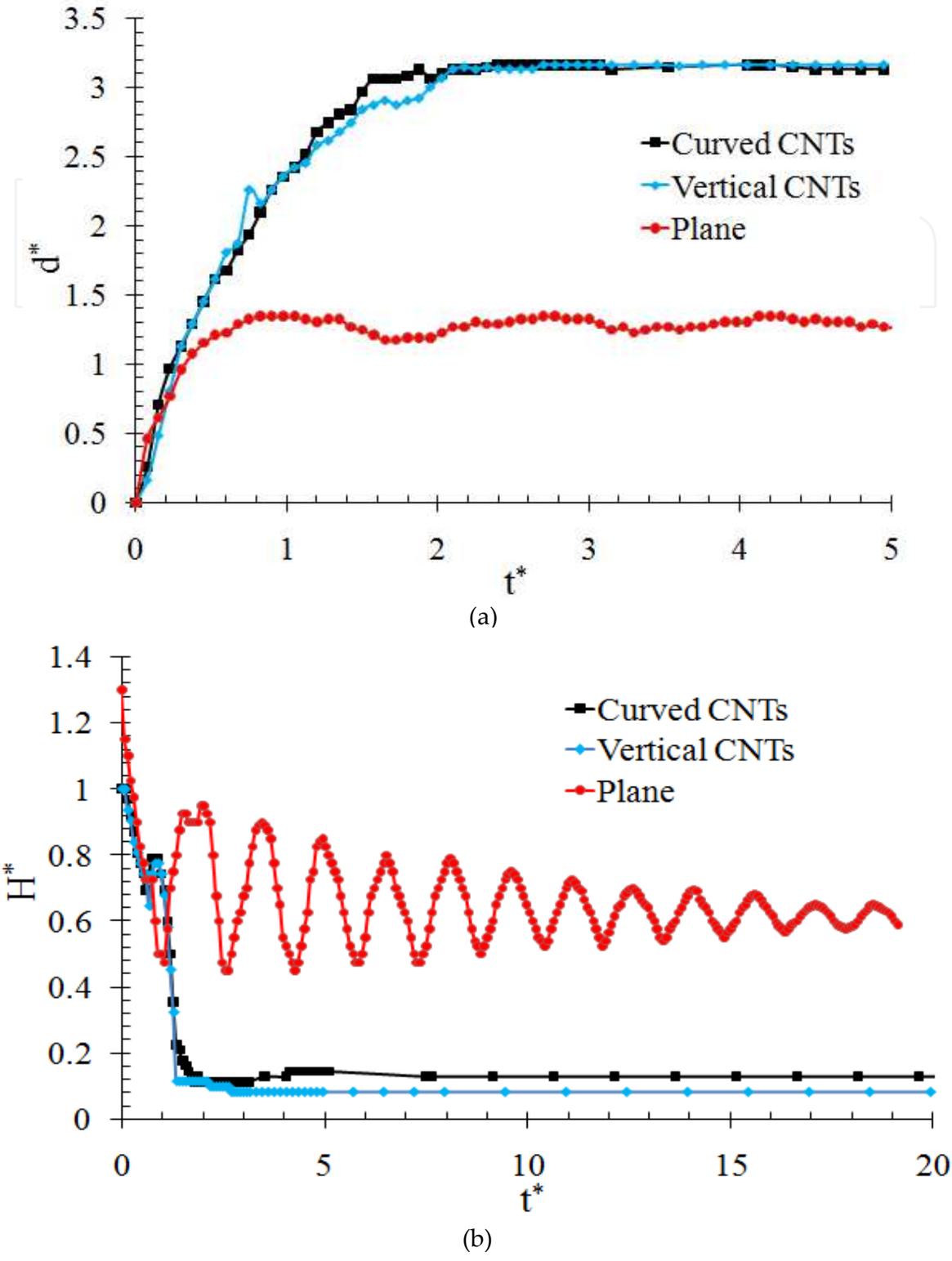



**Figure 9.** Initial impact non-dimensional parameter time evolution illustration at $T_s$=24 °C:(a)$d^*$ [$d/d_o$ ] versus $t^*$[ $t/(d_o/V_o)$],(b) $H^*$[ $H/d_o$] versus $t^*$[ $t/(d_o/V_o)$]

Figure 9(a) shows a rapid initial advancing to a maximum diameter followed by a rebound. The maximum spreading for all cases occurs within $t^*<2$ at $T_s$ = 24°C. Figure 9(b) show that

the droplet height at essentially the same phase oscillating at a 55°contact angle on oxidized silicon surface, where a higher droplet height results in larger contact angles. These results indicate that the surface energy differences are enhanced somewhat for the nanotextured surface with a reduction of the relative advancing and receding contact angles during the initial impact. Also, the contact angle oscillations that occur once spreading has come to equilibrium seem to be damped. Image of water impingement on three surfaces with boiling are shown in figure 10, where (a)-(c) are the images corresponding to the full-drop bouncing back. The rebounding surface temperature of oxidized silicon, vertical CNTs and curved CNTs comparison are 165°C, 247°C and 257°C, respectively, for surface temperatures at a heating ($T_s$) and rebounding ($T_r$) condition.

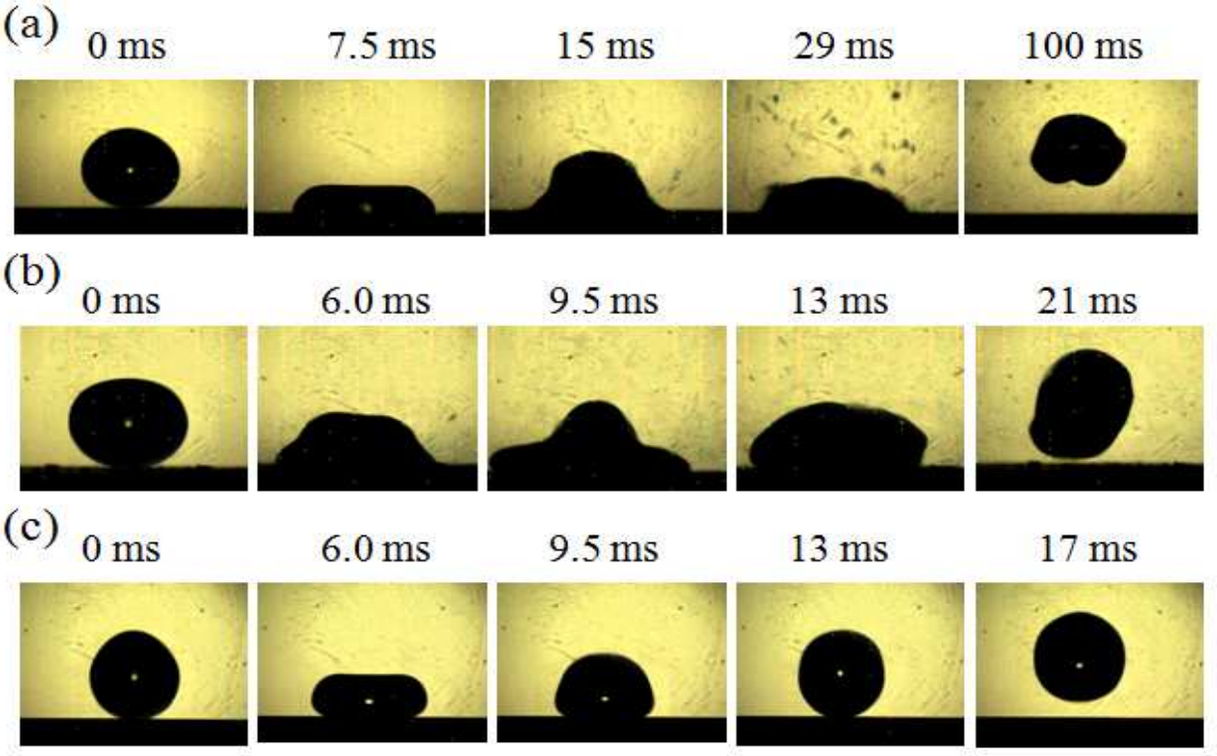



**Figure 10.** Snapshots of free fall droplets released from various surfaces at rebounding temperature ($T_r$):(a) on the oxidized silicon at $T_r$=165°C,(b) on the vertical CNTs surface at $T_r$=247°C, (c)on the curved CNTs surface at $T_r$=257°C .

Results show that the curved wire nanostructured surface enhanced capillary pumping effect and retained water at higher surface temperatures ($T_s$=226°C), as seen in figure 11. During the advancing phase the contact line length is nearly identical for the two nano-textured surfaces, however, during the retraction phase the contact line for the droplet on the curved CNTs at a surface temperature of 248°C becomes pinned, while the droplet on the vertical CNTs at a surface temperature of 248°C retracts and then rebounds off the surface is shown in figure 12. The increased spreading area over the curved CNTs surface suggests a greater potential for increased liquid lateral transportation and retention, thus bring out the consequence in improving high efficiency cooling.

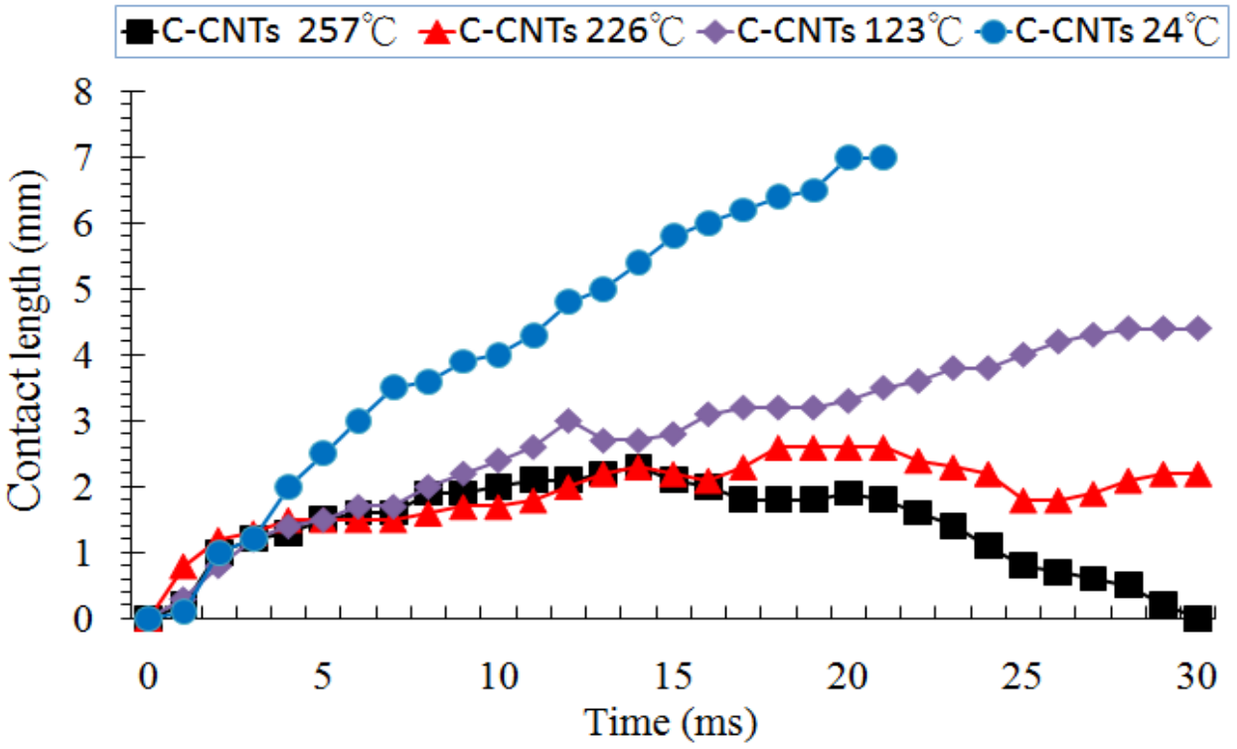



**Figure 11.** Contact line length versus time for droplets impinging on the curved CNTs surface at different temperatures

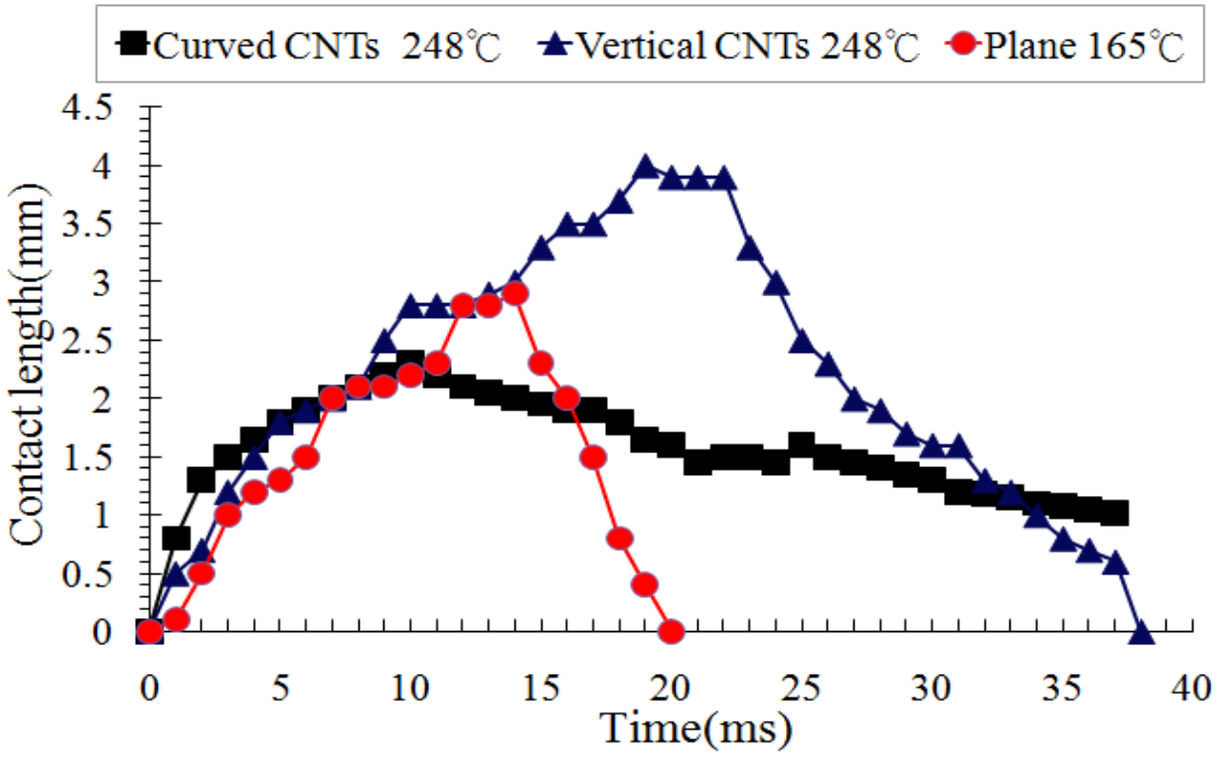



**Figure 12.** Contact line length versus time for droplets impinging on three surfaces at different temperatures

A digital pipette dispensed 0.1~2 μl of water onto CNTs nanotextured surface (hydrophilic surface) because the CNTs surfaces were hydrophilic modification. A 2.0 μl droplet of distilled water is placed on the heat surface at $T_s$=125 °C with three samples of oxidized silicon, vertical CNTs , or curved CNTs, respectively, and the water droplets were extended to a film as a function of very smaller CA was larger. The impact of a distilled water droplet upon a heated surface was investigated experimentally using a high-speed digital camera. Figure 13 illustrates images corresponding to the different characteristic stages of water droplet of 2.0μl evaporation on the oxidized silicon surface for a typical boiling condition. The time of initial solid-liquid contact, i.e. the first significant frame of a series, was taken to be the origin of the time axis ($t_0$ = 0). Thus, the last frame with the droplet still being visible corresponds to the droplet evaporation time. The droplet immediately boils when it contacts the surface, large bubble can be divided into film evaporation and nucleate boiling consequently dry-out are shown in figure 14. The curved CNTs surface enhanced capillary pumping effect and retained water during higher surface temperatures, evaporation rates are high and consequently the droplet lifetimes are short as shown in figure 15.

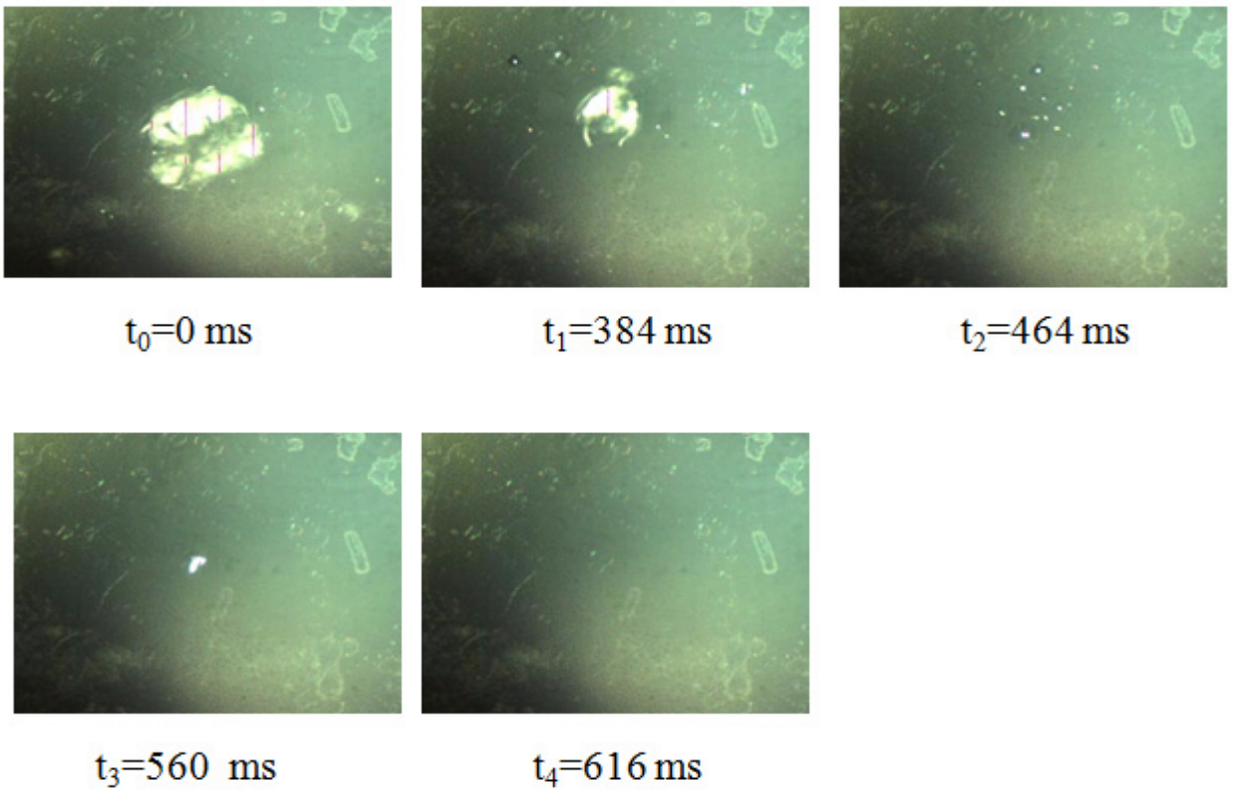



**Figure 13.** Images of top view corresponding to the characteristic stages of the droplet evaporation process for 2 μL water droplet impinging on plane oxidized silicon, typical boiling condition, Ts = 125 °C.

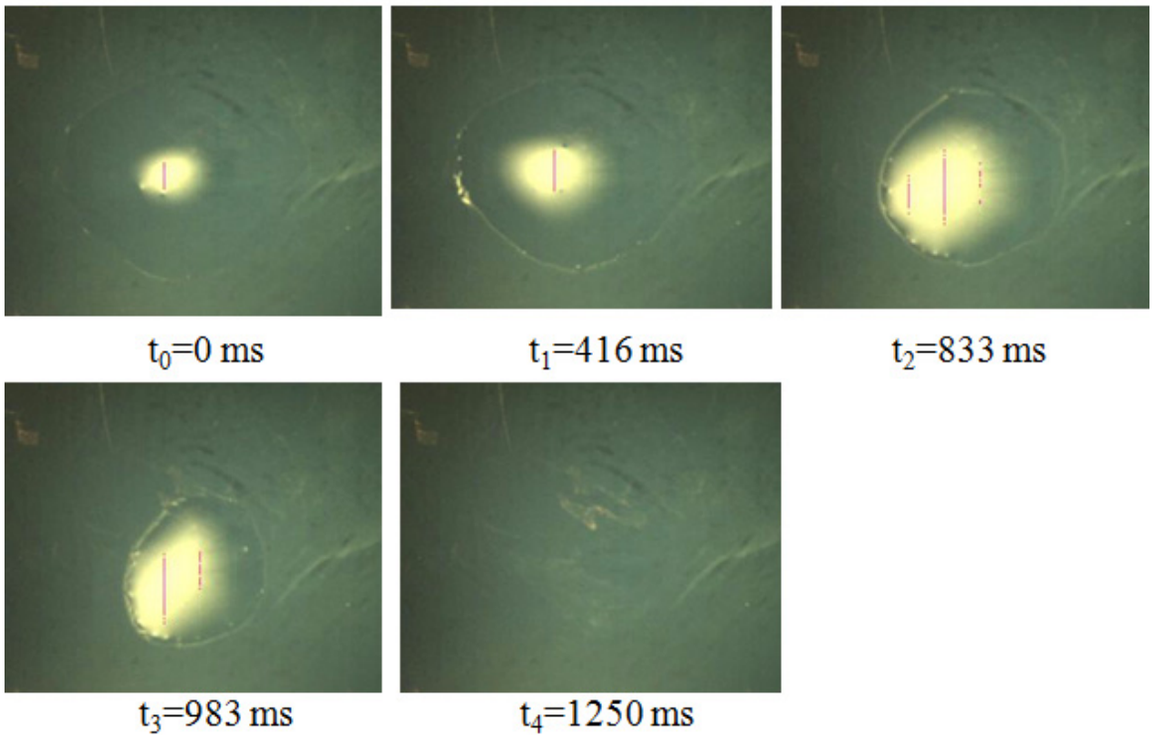



**Figure 14.** Images of top view corresponding to the characteristic stages of the droplet evaporation process for 2 μL water droplet impinging on the vertical CNTs surface, typical boiling condition, Ts = 125 °C.

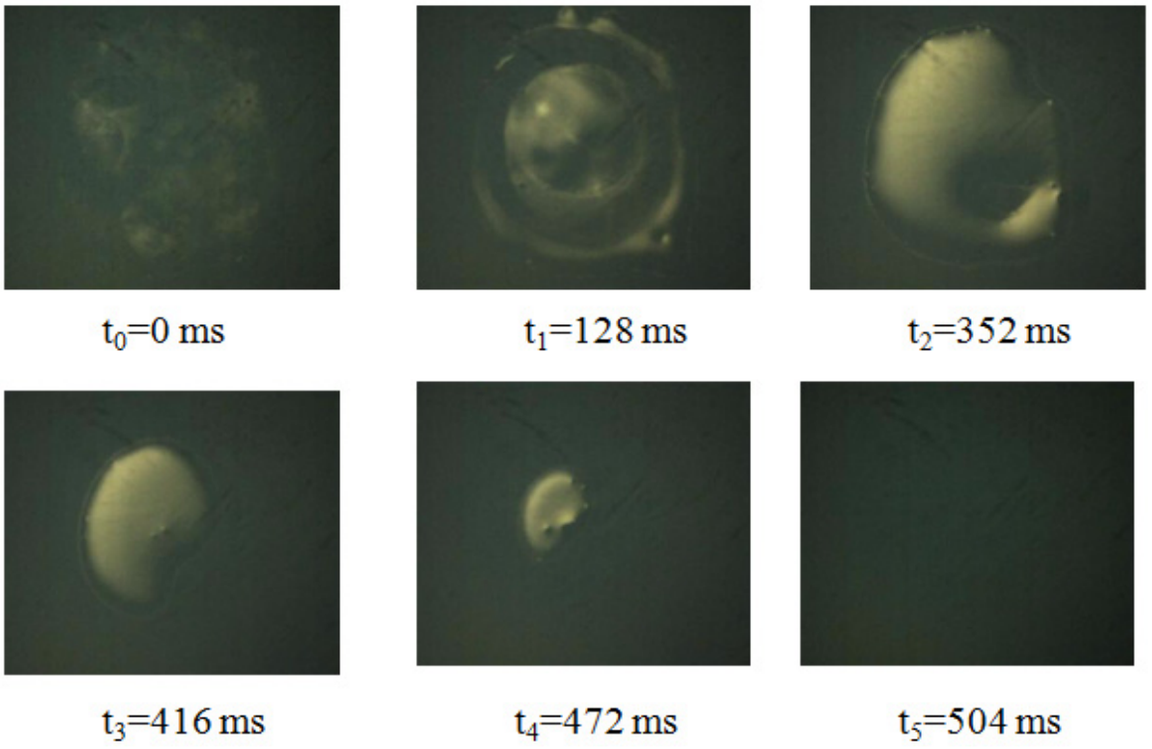



**Figure 15.** Images of top view corresponding to the characteristic stages of the droplet evaporation process for 2 μL water droplet impinging on the curved CNTs surface, typical boiling condition, Ts = 125 °C.

Figure 16 show the heat transfer curves of water spray cooling on the oxidized silicon and nanotextured surfaces when the cooling liquid is sprayed at a constant flow rate (11.7 ml/min) and standard ambient pressure (1 atm). In the evaporative zone, the heat flux range of 30~40 W/cm², the mean heat transfer coefficient of the curved CNTs surface was approximately 140% higher than that of the plane surface. Figure 17 shows the heat transfer coefficient with heat flux. The heat transfer coefficient derived from Eq. 1. The heat transfer coefficient of the spray cooling curve has a peak in the evaporative zone, and then, near 15 W/cm², it rapidly decreases. The maximum heat transfer coefficient occurs at curved CNTs surface because the effect of the evaporative latent heat increases to enhance heat transfer. In addition, the heat transfer coefficients of the CNTs nanotextured surface are in the range of 10~25 W/cm², which is higher than that of the plain surface due to the greater level of liquid wetting in the evaporative zone by spray cooling.

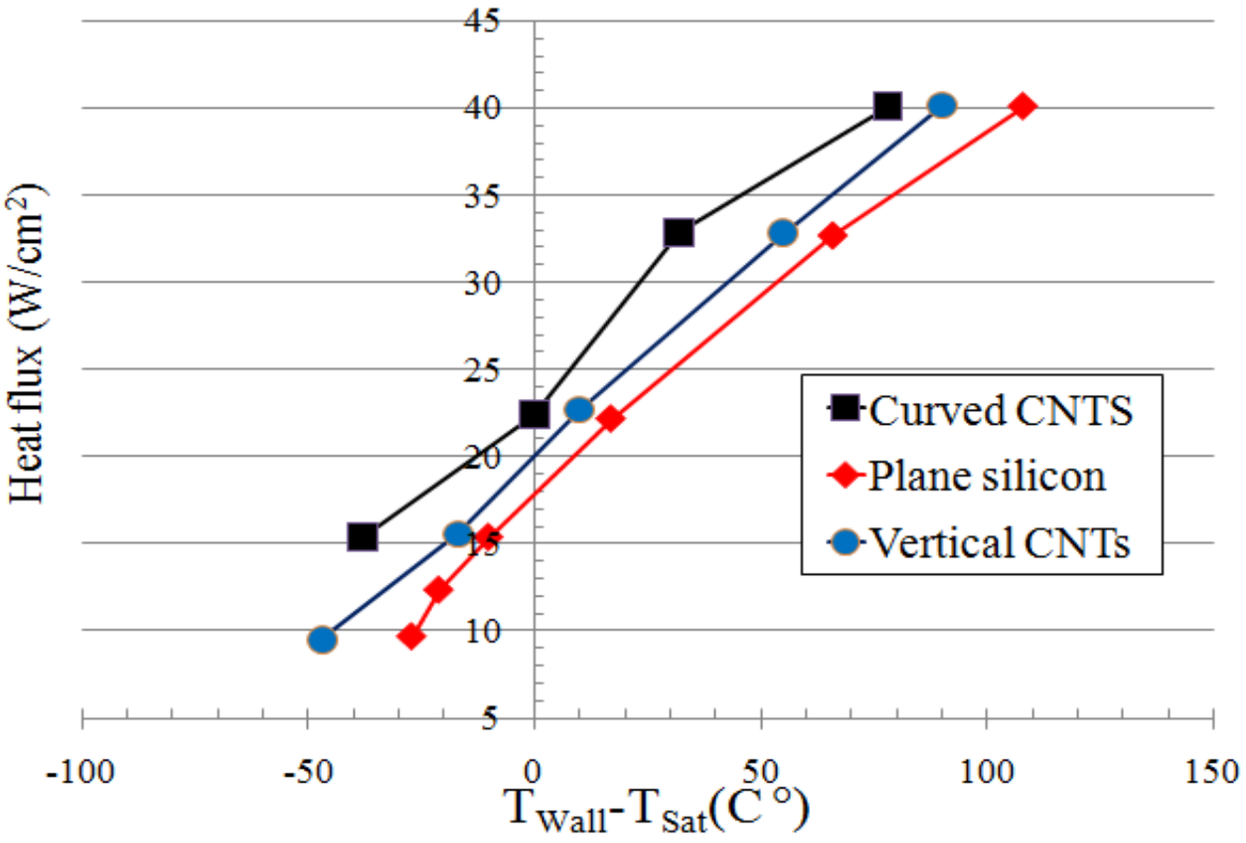



**Figure 16.** Comparison of heat flux between the oxidized silicon and nano-textured surfaces for spray cooling.

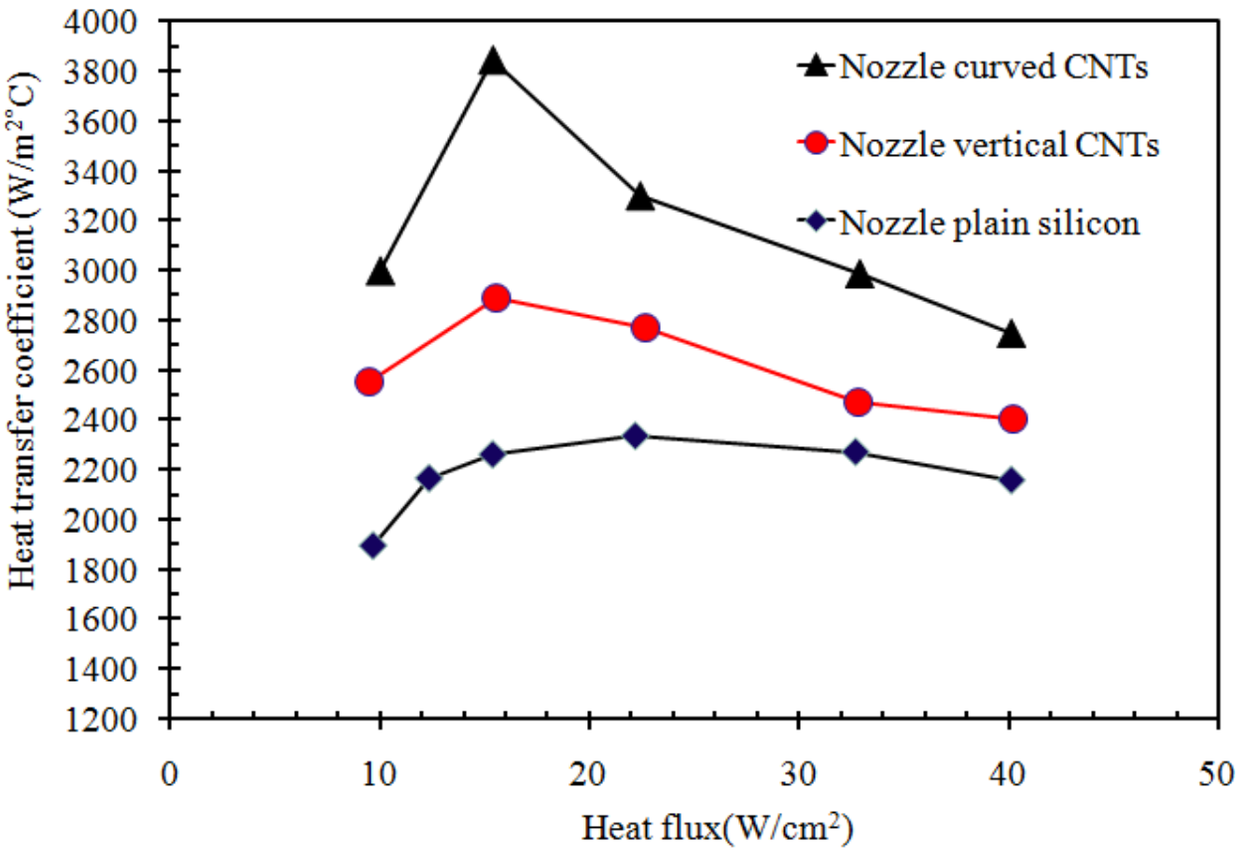



**Figure 17.** Heat transfer coefficients with variations in heat flux between the oxidized silicon and nanotextured surfaces for spray cooling.

## 5. Conclusions

The present study demonstrates the hydrodynamic characteristics of droplet impinging on heated surfaces using high-speed imaging and evaluates the heat transfer performance of surface temperature for water on both plane and nanotextured surfaces. Use of the nanotextured surface have resulted in a more uniform temperature profile at and near the impact area exhibiting lower minimum wall temperature especially at higher heat flux values. Nanotextured surfaces also yield lower static contact angle and enhanced film dynamics resulting in a noticeable enhanced heat transfer behavior. Results show that the curved CNTs surface enhanced capillary pumping effect and retained water during higher surface temperatures. This increased spreading over the nanotextured surface suggests a greater potential for increased liquid transport. In the evaporative zone, the heat flux range of 30~40 W/cm$^2$, the mean heat transfer coefficient of the curved CNTs surface was approximately 140% higher than of the oxidized silicon surface. This study offers insight into the design of nanotextured surface and new opportunities to achieve capillary pumping capability for microfluidic- based thermal management systems.

## Nomenclature

| | |
|---|---|
| $C_p$ | heat capacity (J/kg◎k) |
| d | droplet diameter (mm) |
| $d_o$ | droplet diameter prior to impact (mm) |
| $d^*$ | non-dimensional droplet diameter, $d/d_o$ |
| G | groove width (mm) |
| g | gravitational constant ($N/s^2$) |
| I | Ampere (A) |
| H | droplet height (mm) |
| $H^*$ | non-dimensional droplet height, $H/d_o$ |
| t | time (s) |
| $t^*$ | non-dimensional time, $t/(d_o/V_o)$ |
| $t_{ev}$ | droplet evaporation time (s) |
| T | temperature (°C) |
| $T_r$ | rebounding temperature(°C) |
| $T_s$ | surface temperature(°C) |
| V | voltage (V) |
| $V_o$ | droplet impact velocity (m/s) |

## Greek symbols

| | |
|---|---|
| $\varrho_f$ | fluid density ($kg/m^3$) |
| μ | dynamic viscosity (Pa•s) |
| γ | surface tension (N/m) |
| $\theta$ | contact angle |

## Subscript

| | |
|---|---|
| a | ambient |
| l | liquid phase |
| s | surface |
| v | vapor phase |
| sat | saturation |
| sub | subcooling |
| CHF | critical heat flux |

## Author details

Cheng Lin
*The Second Research Division, Chung-Shan Institute of Science & Technology, Lung-Tan, Taoyan County, Taiwan, R.O.C*

## Acknowledgement

I would like to thank the National Science Council of the Republic of China, Taiwan, for financially supporting this research under Contract No. NSC 99-2221-E-007-028-MY2. The author also wishes to thank the NTHU ESS MEMS Laboratory for use of their facilities.

## 6. References

[1] Bar-Cohen A., Arik, M., and Ohad, M.," Direct liquid cooling of high flux micro and nano electronic components," Proceedings of the IEEE, Vol. 94, No. 8, pp. 1549-1570, 2006.

[2] Berber, S., Kwon, Y.-K., and Tománek, D., "Unusually high thermal conductivity of nanotubes," Phys. Rev. Lett., 84, pp. 4613-4616, 2000.

[3] Silk, E. A., Kim, J. G., Kiger, K. T., "Spray cooling of enhanced surfaces: Impact of structured surface geometry and spray axis inclination", Int. J. Heat Mass Transfer, Vol. 49, pp. 4910-4920, 2006.

[4] Coursey, J. S., Kim, J. G., Kiger, K. T. "Spray cooling of high aspect ratio open microchannels", J. Heat Transfer, Vol. 129, no. 8, pp.1052-1059, 2007.

[5] Pal, A., Joshi, Y.," Boiling of water at sub-atmospheric conditions with enhanced structures: Effect of liquid fill volume", J. Electron. Packag., Vol. 130, no. 1, 011010, 2008.

[6] Ahn, H. S., Sinha, N., Zhang, M., Banerjee, D., Fang, S. K., Baughman, R. H., " Pool boiling experiments on multiwalled carbon nanotube (MWCNT) forests", J. Heat Transfer, Vol. 128, pp. 1335-1342, 2006.

[7] Sodtke C. , Stephan P. ,"Spray cooling on micro-structured surfaces," Int. J. Heat Mass Transfer, Vol. 50, pp. 4089–4097, 2007.

[8] Amon, C.H., Yao, S. C., Wu, C. F. Wu, and Hsieh, C. C., " Microelectro- mechanical system-based evaporative thermal management of high heat flux electronics," ASME Journal of Heat Transfer, Vol. 127, pp. 66-75, 2005.

[9] Hsieh, C. C., Yao, S. C.," Evaporative heat transfer characteristics of a water spray on micro-structured silicon surfaces," Int. J. Heat Mass Transfer, Vol. 49, pp. 962–974, 2006.

[10] Visaria, M. and Mudawar, I.," Application of two-phase spray cooling for thermal management of electronic devices," IEEE Trans. Compon. Packag Technol., vol. 32, no. 4, pp.784–793, 2009.

[11] Ujereh, S., Fisher, T., Mudawar, I.," Effects of carbon nanotube arrays on nucleate pool boiling," Int. J. Heat Mass Transfer, Vol. 50, pp. 4023–4038, 2007.

[12] Li, C., Wang, Z., Wang, P. I., Peles, Y., Koratkar, N., and Peterson, G. P.," Nanostructured copper interfaces for enhanced boiling," Small, Vol. 4, No. 8, pp.1084–1088, 2008.

[13] Chen, R., Lu, M. C., Srinivasan, V., Wang, Z., Cho, H. H. Cho, and Majumdar, A." Nanowires for enhanced boiling heat transfer," Nano Lett., Vol. 9, No. 2, pp. 548-553, 2009.

[14] Khoo, H. S., Tseng, F. G., "Spontaneous high-speed transport of subnanoliter water droplet on gradient nanotextured surfaces", Appl. Phys. Lett., Vol. 95, 063108, 2009.
[15] Chen, M. H., Hsu, T. H., Chuang, Y. J., Tseng, F. G., " Dual hierarchical biomimic superhydrophobic surface with three energy states", Appl. Phys. Lett., Vol. 95, 023702, 2009.
[16] Lin, C., Chen, C. J., Chieng, C. C., Tseng, F. G., "Dynamic effects of droplet impingement on nanotextured surface for enhanced spray cooling ," The 16th International Conference on Solid-State Sensors, Actuators and Microsystems (Transducers'11), Beijing, China, June5-9, pp.1252-1255,2011.
[17] Carey, V. P., "Liquid-vapor phase-change phenomena", Hemisphere: Washington, DC, 1992.
[18] Deng, T., Varanasi, K. K., Hsu, M., Bhate, N., Keimel, C., Stein, J., Blohm, M., "Nonwetting of impinging droplets on textured surfaces", Appl. Phys. Lett., Vol. 94, 133109, 2009.
[19] Mudawar I. and Estes, K. A., "Optimizing and predicting CHF in spray cooling of a square surface," J. Heat Transfer, Vol. 118, pp.672-679, 1996.
[20] Lin, C., Tseng, F. G., Kan, H. C., Chieng, C. C. , " Numerical studies on micropart self-alignment using surface tension forces," J. Microfluidic and Nanofluidic, Vol. 6, pp.63-75, 2009.

IntechOpen